

2 Data Acquisition

Abstract The first step in our pattern classification model design process is presented – data acquisition. We will first introduce the robotic thermal imaging system, consisting of the hardware and software used to acquire thermal data. We will also discuss the methodology used to preprocess and collect our representative data set. The methodology used in our data acquisition is implemented prior to the feature generation step discussed in the next chapter.

2.1 Introduction

In this chapter, we will present the first step in our pattern classification model design process – data acquisition. We will first introduce our robotic thermal imaging system. This system consists of the hardware and software that is used to acquire the image data. We will also discuss the methodology used to preprocess and collect our representative data set prior to the feature generation step discussed in the next chapter.

2.2 Robotic Thermal Imaging System

2.2.1 *Hardware*

The hardware for our robotic thermal imaging system is displayed in Fig. 2.1. Figure 2.1 (a) shows the front view of the robot platform. A metal container encloses the thermal camera to ensure that the camera is on a stable platform and protected from the outside environment. The underside of the adjustable lid on the metal container consists of a polished aluminum plate to reflect thermal radiance

emitted from a target to the thermal camera. The polished aluminum plate is a good reflector of thermal radiation due to its low emissivity value (approximately 0.09 for wavelengths of 8–14 μm) [1]. Consequently, the combination of the thermal camera, metal container, and polished aluminum plate act as a periscope. A Futaba remote control module (displayed in the bottom right corner of Fig. 2.1 (a)) is used to navigate the robot platform.

The thermal camera secured at the bottom of the metal container and displayed in Fig. 2.1 (c) is a *Raytheon ControllIR 2000B* long-wave (7–14 micron) infrared thermal imaging video camera with a 50 mm focal length lens. The key specifications of the *Raytheon ControllIR 2000B* include: 320 X 240 pixel resolution, 30 Hz frame rate, $18^\circ \times 13.5^\circ$ field of view (with 50 mm lens), and ferroelectric staring



Fig. 2.1 Robotic thermal imaging system hardware: (a) robot platform front view, (b) robot platform rear view, (c) Raytheon thermal imaging video camera, (d) VideoAdvantage USB video capture device, (e) Samsung tablet PC w/ Powerbank.

focal plane array detector type. As discussed in Chap. 1, Planck's blackbody radiation law tells us that the magnitude of the radiation emitted by an object varies with wavelength for a given temperature. A perfect emitter (or blackbody) with a surface temperature in the interval from 32° to 100°F radiates a greater magnitude of thermal energy in the wavelength interval of 7–14 microns compared to shorter wavelengths. Therefore, radiation emitted from non-heat generating objects outdoors will peak in the long-wavelength range. In the context of this research, non-heat generating objects are defined as objects that are not a source for their own emission of thermal energy, and so exclude people, animals, vehicles, etc. Consequently, a thermal imaging camera that is sensitive to long-wave thermal radiation is an ideal sensor for our classification application involving non-heat generating objects.

Figure 2.1 (b) displays the rear view of the robot platform. Two metal lockers with hinged doors are stacked behind the "periscope." A *Barnant 90 Digital Thermometer* is attached to the top locker to allow the operator to record the ambient temperature. The bottom locker provides storage for field supplies while the top locker holds a *Samsung Tablet PC* and Powerbank (Fig. 2.1 (e)). *Samsung Tablet PC* has an Intel Celeron 900 MHz processor, 512 MB of RAM, and Microsoft Windows XP Tablet PC Edition operating system. The Powerbank extends the tablet PC's battery life by allowing the operator to continuously capture thermal images for up to approximately 2.5 hours.

The process of capturing a thermal image of a specific target begins with the detectors in the camera's Focal Plane Array (FPA) receiving the thermal radiation emitted from all of the surfaces of objects within the thermal scene. The thermal scene consists of all objects within the camera's field of view, which includes the target of interest and objects in the foreground. In the context of this research, we define foreground as the region in the scene consisting of objects behind the target of interest and within the thermal camera's field of view. Background is defined as the region either in front or to the side of the target consisting of thermal sources that emit thermal energy onto the target's surface. The source emitting this thermal energy may or may not be in the camera's field of view. The thermal radiation received by the FPA is converted to an analog signal with a 320X240 pixel resolution. This analog signal is transmitted from the camera through a harness cable assembly to a *Voyetra Turtle Beach Video Advantage USB Video Capture* device (see Fig. 2.1 (d)) that is attached to the *Samsung Tablet PC*. The *Voyetra Turtle Beach Video Advantage USB Video Capture* device converts the composite analog signal from the camera to a digital signal. The tablet PC receives the digital signal and a thermal image is displayed on the screen using the *VideoAdvantage* software that is installed on the tablet PC, discussed below. A camera control cable also connects the camera to the *Samsung Tablet PC*. The *Control IR Manager* software installed on the tablet PC, discussed in the following section, uses this cable to make modifications to the camera's memory. During thermal image capturing sessions, the door on the top locker is closed to prevent glare on the tablet PC's display screen caused by the sun. With the door shut, the operator views the thermal image on the tablet PC's display screen through the

black eyepiece and captures thermal images with the *VideoAdvantage* software using the mouse, both located on the top locker (see Fig. 2.1 (b)).

2.2.2 *Signal Preprocessing*

In this section, we will discuss the software used to capture and preprocess a thermal image of an object prior to generating features. The significance of preprocessing a thermal image is evident from the thermal image in Fig. 2.2. The quality of this thermal image is affected by temporal and spatial signal degradations and dead pixels. If the magnitude of these typical degradation processes is not minimized, they will have a negative impact on our ability to generate relevant features from the thermal image and characterize unknown objects.

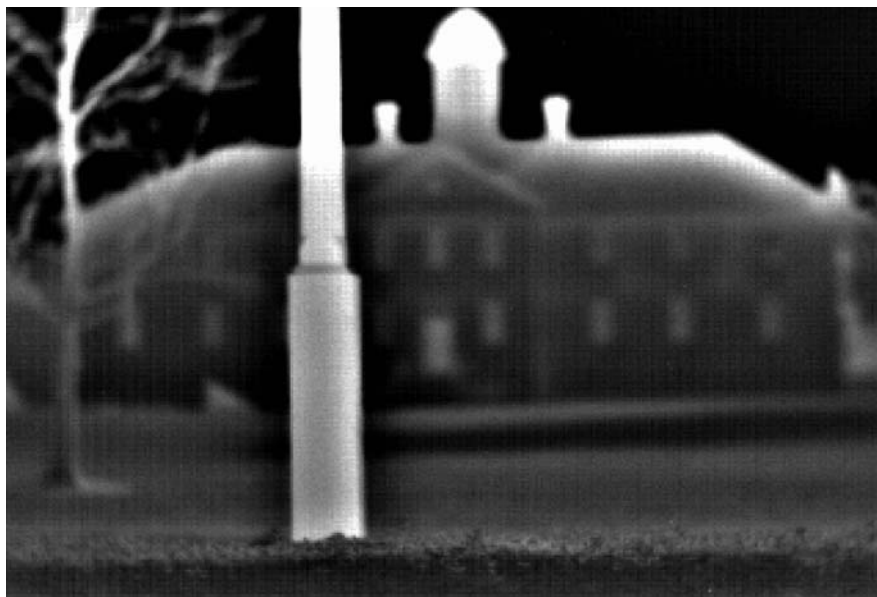


Fig. 2.2 Thermal image prior to preprocessing.

2.2.2.1 *Signal Degradations*

Signal degradations consist of temporal and spatial signal degradations and dead pixels. Temporal signal degradations consist of a temporal fluctuation in the signal at a low frequency (drift), mechanical vibrations due to the movement of camera system relative to the target (jitter), and noise (electronic, optical, and structural) [2, 3]. The spatial signal degradations are displayed as the fine horizontal and vertical lines overlaid on the thermal image in Fig. 2.2. These spatial signal

degradations are due to non-uniformities in the responsivity of the detectors in the FPA [2, 3]. We also see dead pixels (white specks throughout the image) resulting from a defect in the instrumentation caused by events such as heat deterioration or a high incidence of static electricity on a detector [4].

Control IR Manager is software used to control the functionality of the *Raytheon ControlIR 2000B* infrared thermal imaging video camera. The software is used to make modifications to the camera's memory that will preprocess the thermal images and minimize the effects of the degradation processes. We will discuss the key software features used to preprocess our thermal images. Figure 2.3 displays the main menu of the *Control IR Manager* software. The polarity switch in the upper left corner is set to White Hot, resulting in objects with apparent high temperature (hot) surfaces, relative to other objects in the camera's field of view, to yield gray-scale values of 255 (white) in the thermal image. On the other hand, objects that have an apparent low temperature (cold) surface, relative to other objects in the camera's field of view, will yield gray-scale values 0 (black) in the thermal image. Consequently, the thermal radiance emitted from surfaces of objects in the entire scene could result in various gray-scale values in the interval $[0, 255]$. This characteristic of the thermal camera will lead us to an important discussion on AC coupling and the AGC circuit that we will cover shortly.

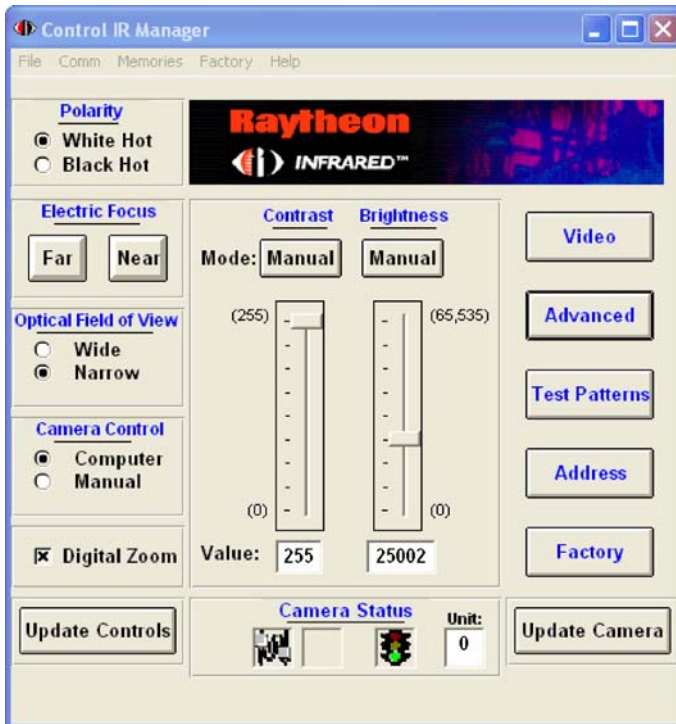


Fig. 2.3 Control IR Manager main menu.

We will now discuss how to make adjustments in the software to suppress the temporal and spatial signal degradations and dead pixels. By selecting the Video icon from the *Control IR Manager* software's main menu (Fig. 2.3) we get the Video Settings menu (Fig. 2.4). By enabling Frame Integration with 16 frames, we can reduce the effects of temporal signal degradations by taking a frame-to-frame average of the scene over 16 frames (the *Raytheon ControlIR 2000B* has a frame rate of 30 Hz). Moving back to the main menu (Fig. 2.3) and selecting the Advanced icon, we go to the Advanced Video Settings menu (Fig. 2.5). By enabling Normalization Correction in the Normalization Options menu, we are able to treat the spatial signal degradations due to the non-uniformity of the detectors in the FPA. Our system uses a single-point non-uniformity correction method that normalizes (makes equal) the outputs for the individual detectors over a uniform thermal scene [5]. In single-point correction, the average of multiple images of a uniform thermal scene (single thermal input intensity or temperature reference) is subtracted from live video to remove the non-uniformity [2, 3]. Also within the Normalization Options menu (Fig. 2.5), we can enable Pixel Substitution to store locations of dead pixels in the FPA and substitute the dead pixels with the mean value of horizontally adjacent good pixels. After suppressing the temporal and spatial signal degradations and dead pixels found in

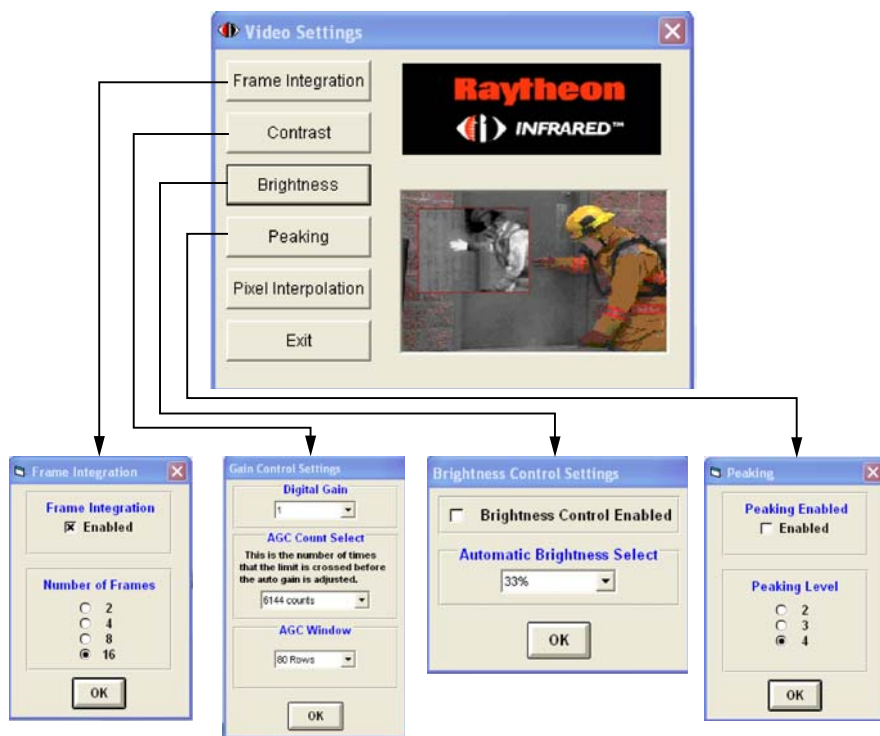


Fig. 2.4 Control IR Manager video settings.

Fig. 2.2, we obtain the resulting thermal image in Fig. 2.6. Table 2.1 presents the procedure to normalize the camera and store the reference in the camera's memory to perform non-uniformity correction on subsequent thermal image frames.

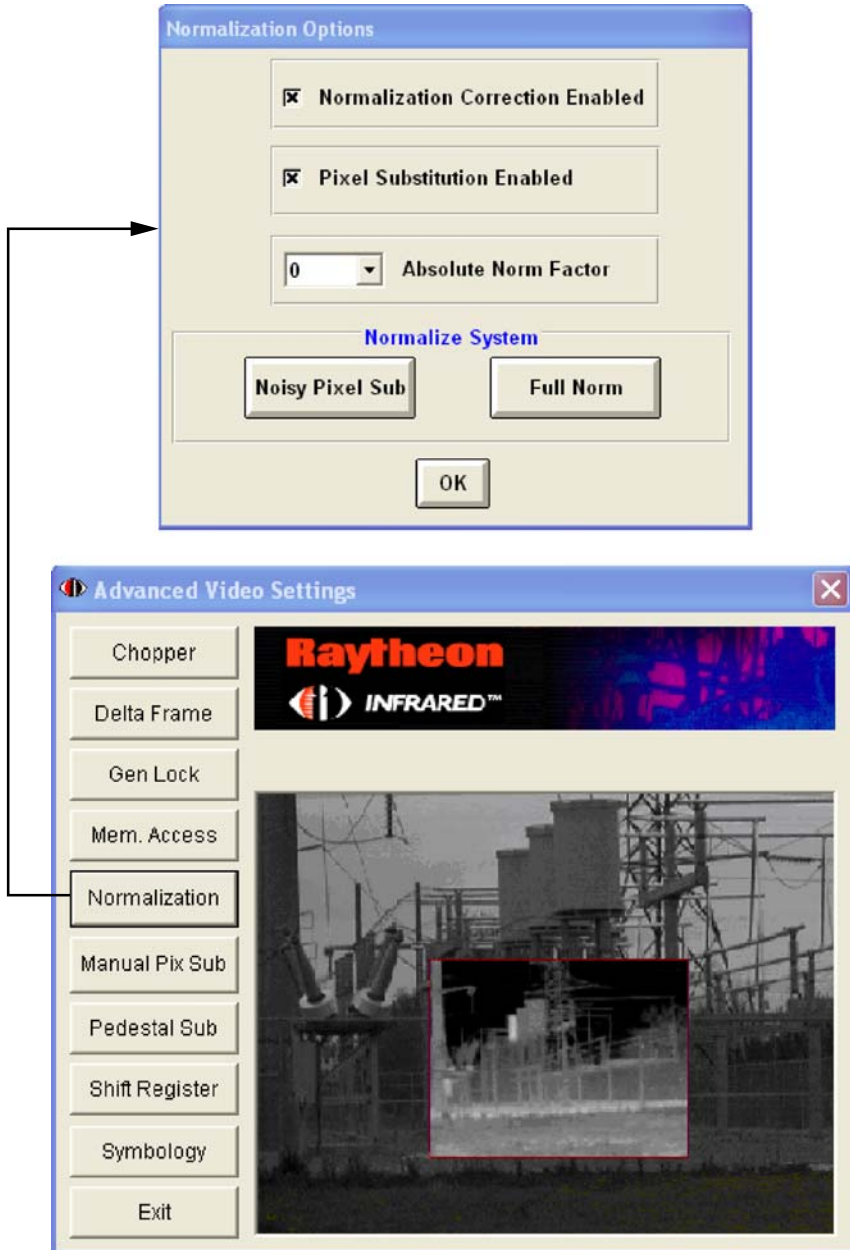


Fig. 2.5 Control IR Manager advanced video settings.

Table 2.1 Procedure to normalize the camera and store the reference in the camera's memory to perform non-uniformity correction on subsequent thermal image frames [5].

- (1) Setup the *Raytheon ControllIR 2000B* approximately 2.5 meters from a smooth, non-shiny, surface with a low thermal reflectivity (i.e., high emissivity), such as plywood with black spray paint on the surface. This uniform surface must take up the entire scene in the camera's field of view.
- (2) Select the Factory icon (Fig. 2.3) and disable Norm Threshold in the Factory Options menu.
- (3) At the main menu (Fig. 2.3), disable Digital Zoom.
- (4) Select the Advanced icon (Fig. 2.3) and the Normalization icon in Advanced Video Settings (Fig. 2.5). Enable Normalization Correction and Pixel Substitution in the Normalization Options menu.
- (5) In the Normalization Options menu (Fig. 2.5), select the Full Norm icon under Normalize System. Run Full Norm for at least 5 minutes and then select Stop.
- (6) At the main menu (Fig. 2.3), enable Digital Zoom.
- (7) Again, in the Normalization Options menu (Fig. 2.5), select the Full Norm icon under Normalize System. Run Full Norm for at least 5 minutes and then select Stop.
- (8) Select the Factory icon (Fig. 2.3) and enable Norm Threshold in the Factory Options menu.

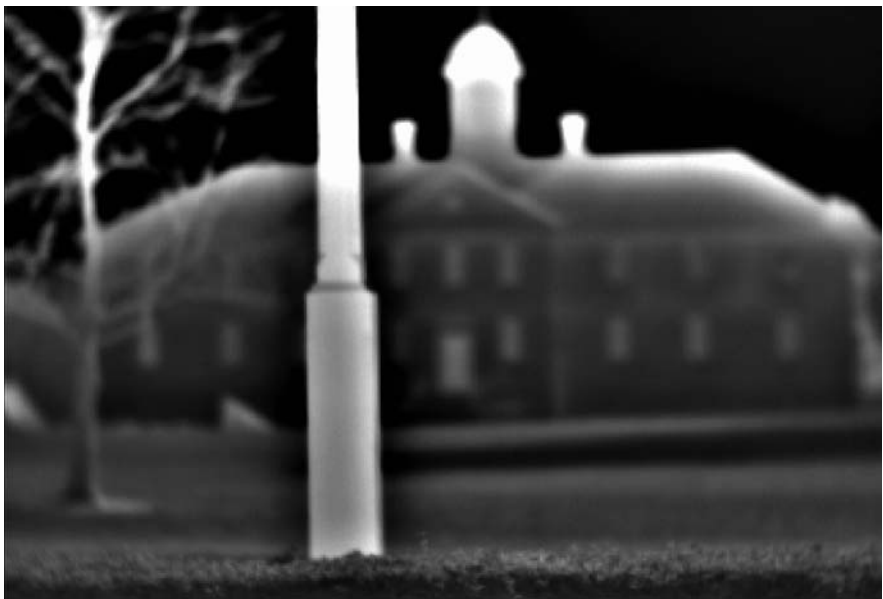


Fig. 2.6 Thermal image with preprocessing on temporal/spatial signal degradations and dead pixels. AGC is enabled.

2.2.2.2 AC Coupling

As mentioned earlier, the polarity for the *Raytheon ControlIR 2000B* was set so the thermal radiance of the surfaces of objects in the entire scene could map to various gray-scale values in the interval $[0, 255]$ where the extremes 0 (black) and 255 (white) imply apparent cold and hot surfaces, respectively. Furthermore, we mentioned that the gray-scale values of an object in a thermal image are assigned relative to other objects in the camera's field of view. This is a characteristic of thermal cameras with FPAs that is known as AC coupling. AC coupling is integrated into the *Raytheon ControlIR 2000B* so that small variations of the surface radiance of objects in a scene can be amplified [1]. Also, a thermal image is AC coupled horizontally along the rows in the image array. A consequence of AC coupling is that a specific target in a scene with a constant thermal radiance could be assigned a large or small gray-scale value depending on the other surfaces in the surroundings within the camera's field of view. Furthermore, a target can only be seen in a thermal image when a thermal contrast exists between the target and other objects in the camera's field of view. Consequently, useful feature values to distinguish objects can only be generated when a thermal contrast exists in the thermal scene. Of course, this makes the objective to classify non-heat generating objects even more challenging since these objects depend highly on prior solar energy absorption in order to emit thermal radiation.

As a result of AC coupling, a target is not radiometrically correct (i.e., the gray-level value is not a linear function of the apparent surface temperature). Figure 2.7 shows an example of AC coupling similar to one illustrated in [1]. Figure 2.7 (a) simulates a scene with uniform thermal physical surface properties (i.e., emissivity, specific heat, etc.) but with different temperature regions. Figure 2.7 (b) displays the resulting thermal image of this scene after AC cou-

"COLD" (75 deg F)	"AMBIENT" (76 deg F)	"COLD" (75 deg F)
"HOT" (77 deg F)		"HOT" (77 deg F)

(a)

Fig. 2.7 (a) AC coupling. Scene with different temperature regions.

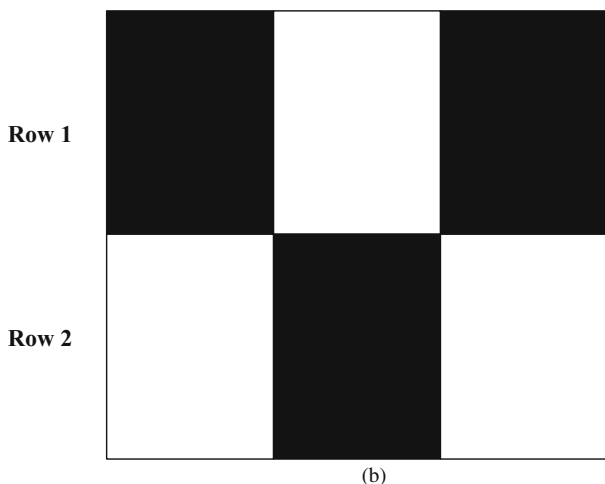


Fig. 2.7 (b) AC coupling. Gray-level shades of regions in thermal image.

pling. As we see, the ambient region maintains a constant temperature of 76°F . However, with AC coupling applied horizontally along the rows in the image, the regions in each row are assigned gray-levels relative to other objects in the same row. As a result, the upper half of the ambient region appears “hot” in Row 1 and the lower half of the ambient region appears “cold” in Row 2.

2.2.2.3 Automatic Gain Control

The effects of AC coupling alone will not hinder our ability to generate features to distinguish objects. However, problems do arise when the amplifications of the gray-level values for an object at a constant temperature become extreme. This issue exists when the *Raytheon ControlIR 2000B*’s automatic gain control (AGC) circuit is enabled. The AGC is an image enhancer that is designed to afford the operator with comfortable image viewing. The AGC automatically adjusts the gain (and offset) to ensure the signals are within the camera’s dynamic range to minimize saturation of objects in the scene [2]. As a result of the AGC, the thermal image of a bright object may be darker and dark object may be brighter. Thus, the AGC amplifies the effects of AC coupling. Similar to AC coupling, the AGC results in gray-level values assigned to objects relative to other objects within a given window. The effects of the AGC circuit are illustrated in Fig. 2.6. Even though the actual surface of the pole is approximately uniform in thermal properties (to include temperature), its thermal image displays an apparent temperature difference between the bottom portion of the pole (with the building in the foreground) and top portion of the pole (with the sky in the foreground).

To investigate the effects of the AGC circuit further, we analyzed variations in gray-level values of a cardboard tube with a constant surface temperature adjacent to

a cardboard tube that is heated to a given temperature and allowed to cool. The cardboard tubes were secured in a thermally insulated box with an opening in the front and a thermal insulator separating the tube on the left (at a constant temperature) from the tube on the right (that was heated). The experiment was conducted in a controlled environment with a constant surrounding radiance and ambient temperature of approximately 59.3°F . The left cardboard tube with a constant surface temperature was maintained at approximately 86.5°F . The surface of the right cardboard tube was heated to 110.8°F and allowed to cool to 65.8°F . Ten images of the scene consisting of the two tubes were captured at increments of approximately 5°F based on the right cardboard tube that was cooling. The mean gray-level values were recorded on the same segments of the two tubes for each image captured. Figure 2.8 illustrates the experimental results with the AGC enabled. Figure 2.8 (a) and 2.8 (b) display the first (right tube at 110.8°F) and tenth (right tube at 65.8°F) images captured, respectively. By comparing Fig. 2.8 (a) and 2.8 (b), we see that the tube on the left (maintained at a constant temperature) varies in gray-levels due to the AGC. Figure 2.8 (c) displays the variations of the gray-levels for the constant and heated tubes as a function of temperature. With the AGC enabled, the constant tube has a standard deviation of 13.84 and range of 44.98 in the gray-levels. Consequently, these extreme variations in gray-level values for the constant tube would hinder our ability to generate relevant features to distinguish objects. Fortunately, we can make modifications to the *Raytheon ControlIR 2000B*'s memory, using the *Control IR Manager* software, to disable the AGC by following the procedure presented in Table 2.2.

We conducted another experiment under the same conditions as described above with the cardboard tubes, with the exception that the AGC was disabled. Once again, the left cardboard tube with a constant surface temperature was maintained at approximately 86.5°F . The surface of the right cardboard tube was heated to 110.4°F and allowed to cool to 65.8°F . Ten images of the scene consisting of the two tubes were captured at increments of approximately 5°F based on the right cardboard tube that was cooling. Figure 2.9 illustrates the experimental results with the AGC disabled. Figure 2.9 (a) and 2.9 (b) display the first (right tube at 110.4°F) and tenth (right tube at 65.8°F) images captured, respectively. By comparing Fig. 2.9 (a) and 2.9 (b), we see that the tube on the left (maintained at a constant temperature) appears to have minimal variation in gray-levels when the AGC is disabled. Figure 2.9 (c)

Table 2.2 Procedure to disable AGC by making modifications in the *Raytheon ControlIR 2000B*'s memory using the *Control IR Manager* software [5].

- (1) In the Video Settings menu (Fig. 2.4), select the Contrast icon to display the Gain Control Settings. Set the Digital Gain equal to 1, AGC Count Select to 6144 counts, and AGC Window to 80 Rows.
- (2) In the Video Settings menu (Fig. 2.4), select the Brightness icon to display Brightness Control Settings. Disable the Brightness Control.
- (3) In the Control IR Manager main menu (Fig. 2.3), set the Contrast Mode to Manual with a Value of 255 and Brightness Mode to Manual with a Value of 25002.

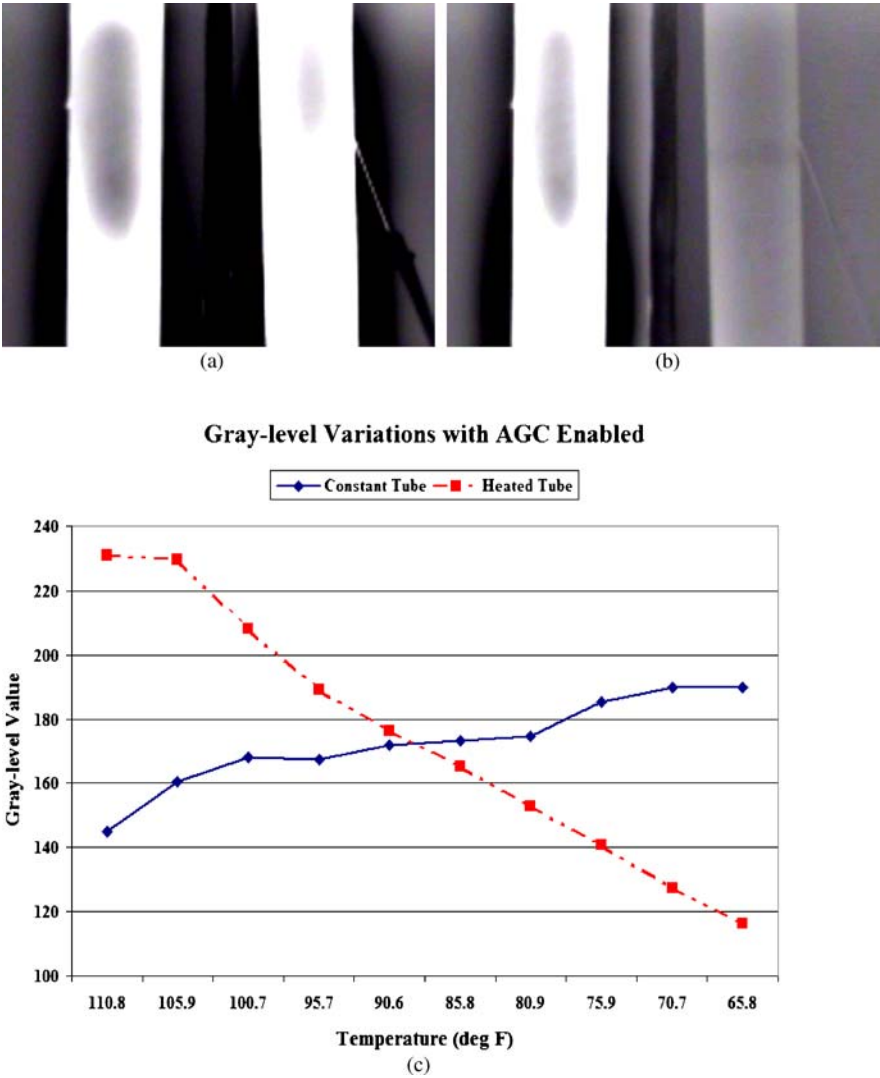


Fig. 2.8 Enabled AGC experiment with cardboard tubes (left tube at constant temperature of ~86.5 deg F and right tube heated to 110.8 deg F and allowed to cool to 65.8 deg F). (a) Image of tubes with right (heated) tube at 110.8 deg F, (b) Image of tubes with right (heated) tube at 65.8 deg F, (c) Variations of gray-levels of constant and heated tubes as a function of temperature.

displays the variations of the gray-levels for the constant and heated tubes as a function of temperature. With the AGC disabled, the constant tube has a standard deviation of 2.16 and range of 7.22 in the gray-levels. Thus, by disabling the AGC, the variations in the gray-level values for the constant tube are only due to AC coupling. Furthermore, by disabling the AGC, the thermal image of the pole displayed in Fig. 2.6 now provides acceptable results for the variation of gray-levels as displayed

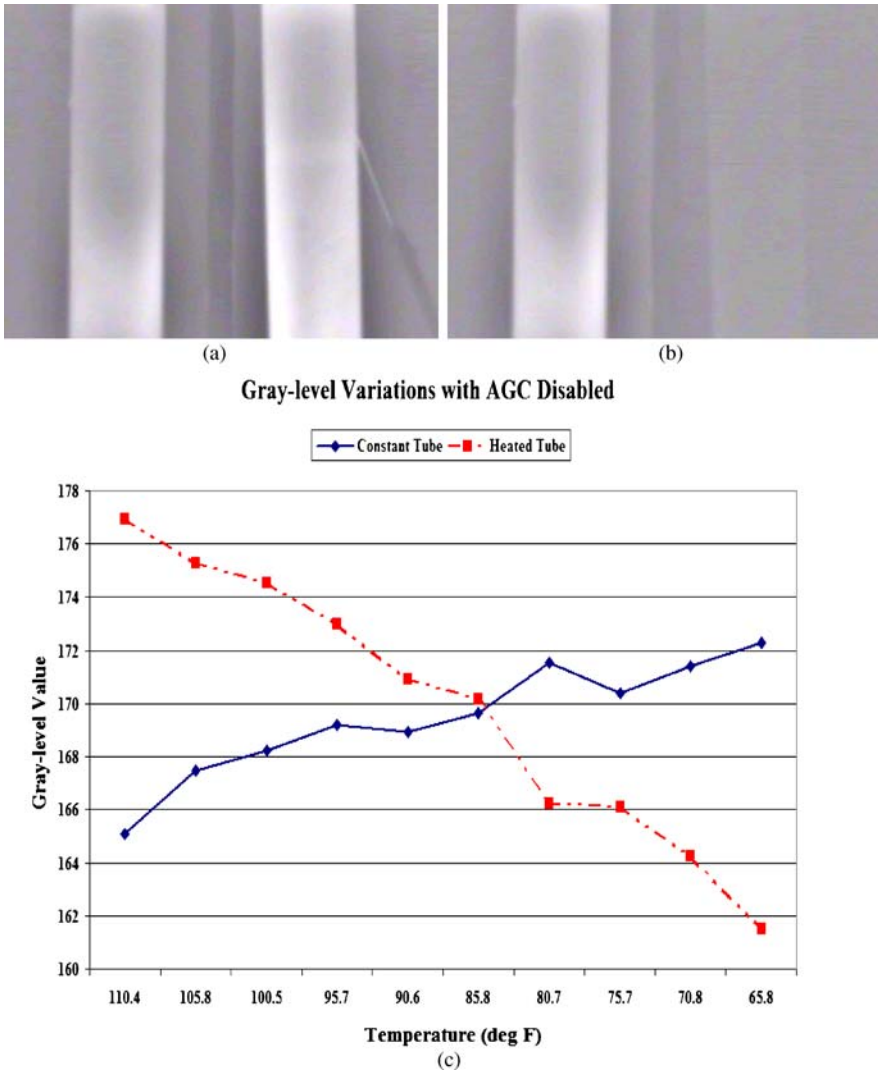


Fig. 2.9 Disabled AGC experiment with cardboard tubes (left tube at constant temperature of ~ 86.5 deg F and right tube heated to 110.4 deg F and allowed to cool to 65.8 deg F). (a) Image of tubes with right (heated) tube at 110.4 deg F, (b) Image of tubes with right (heated) tube at 65.8 deg F, (c) Variations of gray-levels of constant and heated tubes as a function of temperature.

in Fig. 2.10. Therefore, with the AGC disabled we can now generate relevant features from the thermal images of objects that will assist us in classifying the objects.

At this point it is appropriate to mention the halo effect around the bottom portion of the pole in Fig. 2.6. The halo effect is common with ferroelectric FPAs where accurate imagery is assisted by a mechanical chopper wheel within the camera. As discussed in [6], capturing a thermal image of a target is a cyclic process.



Fig. 2.10 Thermal image with preprocessing on temporal/spatial signal degradations and dead pixels. AGC is disabled.

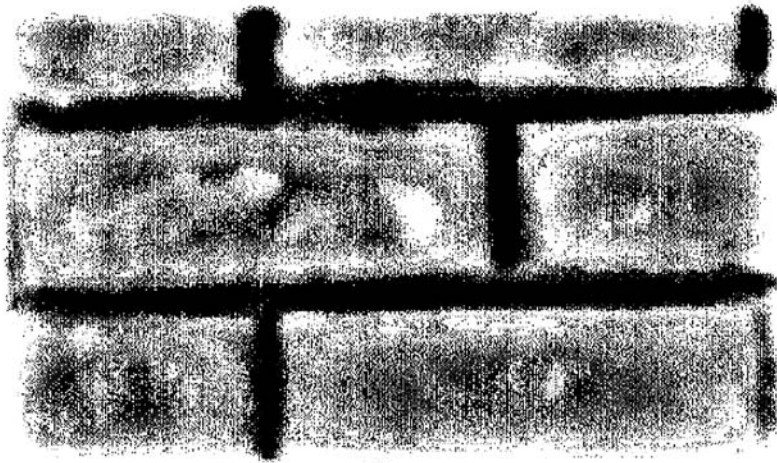
Suppose the target is emitting more thermal radiation than any other neighboring object in the scene (either directly adjacent or behind the target). To capture a thermal image, the target first emits radiation onto the back of the chopper wheel and the FPA obtains a charge reading from the wheel. Next, the FPA obtains a charge directly from the actual target emitting the thermal radiation. Lastly, the system electronically subtracts the charges with and without the chopper wheel to produce the thermal image. However, the thermal radiation from the hot target that leaks through the camera's chopper wheel is unfocused, leaving a larger radiation imprint on the FPA than that of the actual target. When the system subtracts the charges with and without the chopper wheel, a halo is created around the "hot" target in the image that is darker than the "cold" foreground. As we will see in Chap. 3, a "cold" target and "hot" foreground will result in a halo around the "cold" target that is a lighter shade than the "hot" foreground. Fortunately, the halo effect will not interfere with our ability to generate thermal features for classifying objects. As a matter of fact, we will discuss in Chap. 6 how we may be able to use the halo effect to facilitate the segmentation of targets [7].

2.2.2.4 Filters

One of our goals in preprocessing is to suppress degradations in the signal without losing information that would assist in classifying objects in the scene. Consequently, we avoid filters that would lead to loss of relevant information used to distin-



(a)



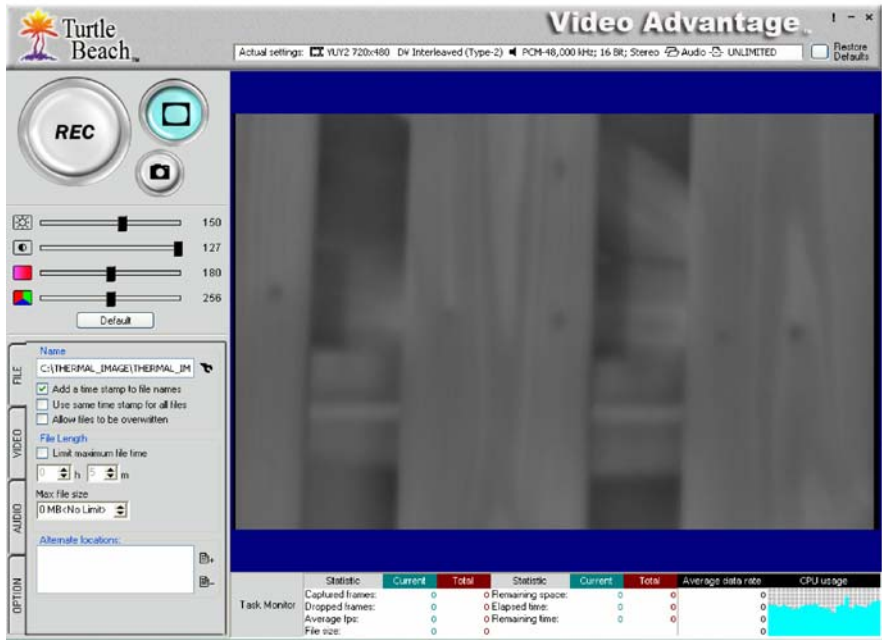
(b)

Fig. 2.11 Thermal image of segment of brick wall: (a) without high pass filter, (b) with high pass filter.

guish object classes. For example, in the Video Settings menu (Fig. 2.4) of the *Control IR Manager* software we disable Peaking since this functionality performs a high-pass filter on the thermal image. Figures 2.11 (a) and (b) display thermal images of the same segment of a brick wall without and with a high pass filter, respectively. As we see in Fig. 2.11 (b), applying a high pass filter results in a loss of information that could be used by thermal features to classify objects.



(a)



(b)

Fig. 2.12 (a) Robotic thermal imaging system capturing an image of a wood fence. (b) Thermal image of the wood fence displayed with *Video Advantage* software.

2.2.2.5 Capturing Thermal Imagery

After the analog signal from *Raytheon ControlIR 2000B* is converted to a digital signal by the *Voyetra Turtle Beach Video Advantage USB Video Capture*, the *Samsung Tablet PC* receives the digital signal and a thermal image is displayed on the screen using the *VideoAdvantage* software. Figure 2.12 illustrates a scenario with the robotic thermal imaging system capturing an image of a segment of a wood fence. The *VideoAdvantage* software displays live video and is capable of capturing continuous or still frames. Our current research will focus on classifying non-heat generating objects in thermal images using still frames. However, we intend to extend our research to classify objects using continuous frames as discussed in Chap. 6. The final preprocessing step before the feature generation phase is to convert the RGB (red, green, blue) image captured by the *VideoAdvantage* software to a gray-scale image using MATLAB.

2.3 Data Collection

We now present the methodology used to collect the data needed to train and evaluate our pattern classification model. We assume that the robot already makes use of algorithms to detect and segment a specific target, analogous to those discussed in Chap. 1. In Chap. 6, we will discuss possible techniques for automated detection and segmentation of objects that we intend to integrate into our future research. Consequently, in the current research we will manually segment our targets.

Thermal imagery was captured on a variety of non-heat generating outdoor objects during a nine-month period, at various times throughout the days and at various illumination/temperature conditions. The ambient temperature (in degrees Fahrenheit) was recorded during each session. The images were captured using a *Raytheon ControlIR 2000B* long-wave (7–14 micron) thermal infrared imaging video camera with a 50 mm focal length lens at a distance of 2.4 meters from the given objects. The analog signals with a 320 X 240 pixel resolution were converted to digital signals using a *Voyetra Turtle Beach Video Advantage USB Video Capture* device attached to a *Samsung Tablet PC*, all mounted on board a mobile robotic platform displayed in Fig. 2.1. The resulting digital frames were preprocessed as discussed in Sect. 2.2.

The image data was divided into two categories: extended objects and compact objects. The extended objects consist of objects that extend laterally beyond the thermal camera's lateral field of view. Our classes of extended objects consist of brick walls, hedges, wood picket fences, and wood walls. The compact objects consist of objects that are completely within the thermal camera's lateral field of view. Our classes of compact objects consist of steel poles and trees. The image data collected was partitioned into three mutually exclusive sets: training data, test data, and blind data. The training data was used to design our pattern classification model. The performance of the model was assessed using the test and blind

data sets. Since the test set was used as a validation set to tune the pattern classification model, it was part of the training process and not being used to provide an independent error estimate. Therefore, the blind data set was used for our independent performance evaluation of the pattern classification model.

Our objective is to design a pattern classification model that displays exceptional performance in classifying unknown non-heat generating objects in an outdoor environment. To satisfy this objective, the data that we collect must completely and accurately represent the real world problem by consisting of all the meaningful variations of field data instances that the system is likely to encounter. Thus, our representative data was collected under diverse environments (climates), temperatures, solar energy conditions, and viewing angles.

Figures 2.13 and 2.14 display the visible and typical thermal images of extended and compact objects, respectively, used for our training data that was collected from 15 March to 22 June 2007 about The College of William & Mary campus. The strips of black electrical tape shown in the visible images and displaying a high thermal radiance in some of the thermal images are used as a reference emitter for generating the thermal features that we will discuss in Chap. 3. During each of the 55 sessions, the thermal images were captured on each object from two different viewing angles: normal incidence and 45 degrees from incidence. Table 2.3 and Fig. 2.15 present the frequencies of the object classes and ambient temperature distribution for the training data, respectively.

The thermal images used for the test data consisted of the same objects used in the training data (Figs. 2.13 and 2.14). The thermal images were captured at the same viewing angles as the training data. However, the test data was collected over nine sessions from 25 June to 3 July 2007. Table 2.3 and Fig. 2.15 present the frequencies of the object classes and ambient temperature distribution for the test data, respectively.

The blind data set was collected over 14 sessions from 6 July to 5 November 2007. The thermal images used for the blind data set consisted of the same classes and were captured at the same viewing angles as the training data but were not the same objects. In addition to some blind data being collected on The College of William & Mary campus, data was also collected throughout York County, Virginia, in a village and on a farm outside Buffalo, New York, and on mountainous terrain in Eleanor, West Virginia. Table 2.4 presents the frequencies of the objects in the blind data set as well as the locations that the data was collected. Figure 2.15 displays the ambient tem-

Table 2.3 Distribution of training and test data collected from 15 March to 3 July 2007.

DATA TYPE	OBJECT CLASSES						Total
	Extended Objects				Compact Objects		
	Brick Wall	Hedges	Picket Fence (Wood)	Wood Wall	Steel Pole	Tree	
Training	105	107	107	105	318	318	1060
Test	18	16	16	18	48	52	168



Fig. 2.13 Visible and thermal images of extended objects from the training data set. (a) brick wall, (b) hedges, (c) wood picket fence, and (d) wood wall.



Fig. 2.14 Visible and thermal images of compact objects from the training data set. Steel poles: (a) brown painted surface, (b) green painted surface, (c) octagon shape w/ aged brown painted surface. Tree: (d) basswood tree, (e) birch tree, (f) cedar tree.

perature distribution of the blind data set. Additionally, to evaluate the classification model’s response when confronted with other blind objects, to include objects outside the classes in the training data set, we included data consisting of a brick wall with moss on the surface, concrete wall, bush, gravel pile, steel picket fence, wood bench, wood wall of a storage shed, square steel pole, aluminum pole for a dryer vent, concrete pole, knotty tree, telephone pole, 4×4 wood pole, and pumpkin.

Table 2.4 Distribution of blind data collected from 6 July to 5 November 2007.

	OBJECT CLASSES						
	Extended Objects				Compact Objects		
LOCATION	Brick Wall	Hedges	Picket Fence (Wood)	Wood Wall Fence	Steel Pole	Tree	Total
New York	3	4	10	3	1	7	28
William & Mary	16	10	9	14	2		51
West Virginia						1	1
York County	4	9	4	6	17	12	52
Total	23	23	23	23	20	20	132

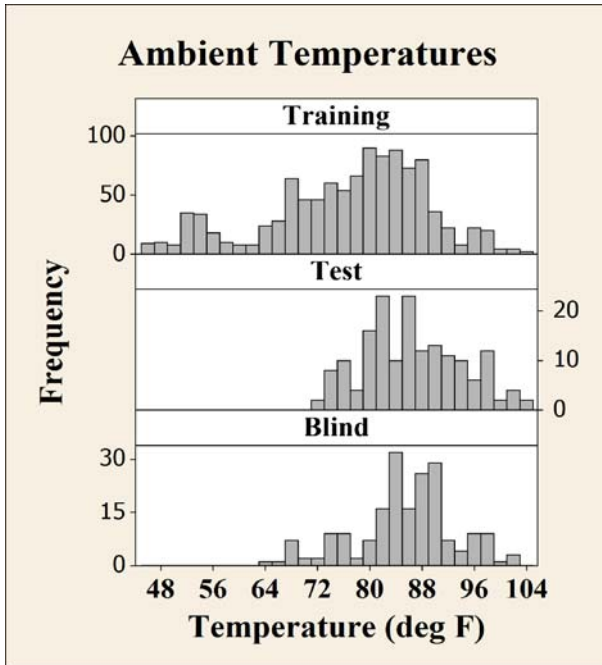


Fig. 2.15 Ambient temperature distributions for training, test, and blind data collected from 15 March to 5 November 2007.

2.4 Summary

In this chapter, we discussed the first step in our pattern classification model design process – data acquisition. We introduced our robotic thermal imaging system consisting of the hardware and software used to acquire thermal data. We also discussed the methodology used to preprocess and collect our representative data set. The methodologies used in our data acquisition are implemented prior to the feature generation step discussed in the next chapter.

References

- [1] Holst GC (2000) Common Sense Approach to Thermal Imaging. JCD Pub.; co-published by SPIE Optical Engineering Press, Winter Park, Fla.; Bellingham, WA
- [2] Holst GC (1998) Testing and Evaluation of Infrared Imaging Systems. 2nd edn. JCD Pub.; SPIE Optical Engineering Press, Winter Park, FL; Bellingham, WA
- [3] Maldague XPV (2001) Theory and Practice of Infrared Technology for Nondestructive Testing. Wiley, New York

- [4] Ginesu G, Giusto DD et al (2004) Detection of Foreign Bodies in Food by Thermal Image Processing. *IEEE Transactions on Industrial Electronics* 51(2):480–490
- [5] Private Conversation with Field Application Engineer, L-3 Communications Infrared Products, 27 January 2007.
- [6] Pandya N, Van Anda J (2004) Across the Spectrum. *SPIE's Oemagazine* :28–31
- [7] Goubet E, Katz J et al (May 2006) Pedestrian tracking using thermal infrared imaging. *Proceedings of SPIE, Infrared Technology and Applications XXXII*:62062C-1 - 62062C-12



<http://www.springer.com/978-1-84882-508-6>

Mobile Robot Navigation with Intelligent Infrared Image
Interpretation

Fehlman, W.L.; Hinders, M.K.

2009, XXIX, 274 p., Hardcover

ISBN: 978-1-84882-508-6